# Design and Analysis of CMOS-Controlled Tunable Photodetectors for Multiwavelength Discrimination

Ray Chen, *Member, IEEE*, Junxian Fu, *Member, IEEE*, David A. B. Miller, *Fellow, IEEE*, and James S. Harris, Jr., *Fellow, IEEE*

***Abstract*—In this paper, a metal–semiconductor–metal (MSM) based photodetector for multiple wavelength discrimination is fully introduced and analyzed. Its spectral response is programmable electrically through a set of low-voltage binary patterns that can be generated from CMOS circuits. Consequently, the wavelength reconfiguration time of the detector is set primarily by the electronics switching time, which is on the order of nanoseconds. Additionally, the spectral response of the detector can be arbitrarily shaped for any specific system need based on algorithms we introduce here. The nanosecond wavelength reconfigurability feature of the detector offers flexibility for designing high-efficiency wavelength reconfigurable optical networks.**

***Index Terms*—Dense wavelength-division multiplexing (DWDM), metal–semiconductor–metal (MSM) photodetector, optical access network, optical code division multiple access (OCDMA), optical sensing, passive optical network (PON), reconfigurable WDM network, telecommunication, tunable photodetector.**

## I. Introduction

Wavelength-division multiplexing (WDM) is a promising technique to share the large fiber bandwidths among many users. In order to leverage the resources of WDM networks in an efficient and flexible manner, incorporating dynamic wavelength allocation in the WDM networks is very beneficial. In addition to the reconfigurability of WDM networks, packet switching is another trend for future networks. Incorporating dynamic wavelength allocation in the packet-switching network can further utilize the network resources in a much more efficient, flexible, and robust manner. Combining the two future trends together to perform packet-based wavelength tuning, the wavelength transition time between two adjacent packets needs to be much shorter than the packet length. For a packet that is of microsecond length, the transition time needs to be in a nanosecond scale. Unfortunately, wavelength-switching access times of all of the currently available tunable filters and photodetectors are relatively slow, ranging from a few seconds to a few microseconds, depending on the device's working principle [1]. For example, acoutsto-optical tunable filters (AOTFs) have microsecond tuning time [2]. Microelectromechanical system (MEMS) based tunable filters usually have millisecond tuning time and require tens of volts to bias, which prohibit their integration with CMOS electronics [3]. Thermally tuned filters usually have millisecond tuning time and are definitely temperature-sensitive [4]. Intrinsic-absorption-based tunable photodetectors have the potential to tune fast. (Intrinsic-absorption-based detectors refer to devices whose photon absorption process and spectrum are based on a physical property of the device, as in, for example, electrically biased quantum wells.) However, the tuning range of such intrinsic-absorption-based devices is small and they usually require large biasing voltages to achieve the absorption contrast ratio specification of systems [5]; these large voltages also inhibit intimate integration with CMOS control electronics. Besides, their spectral responses are less easy to shape for specific system applications. For the new device that will be introduced in this paper, the spectral response can be simply retrimmed/reshaped in arbitrary forms for specific system needs simply by applying another low-voltage binary pattern. The low-voltage binary biasing feature significantly reduces the design complexity of the driver circuits, which means that no delicate analog electronics is needed.

To understand the operation of the device, we have to first understand the optics associated with it. Most of the optical devices that can discriminate one wavelength from others either have external optical wave interferences or resonators, or have internal resonant transitions (e.g., quantum mechanical transition energies or bandgaps). For the external optical approaches, the incoming signal interferes with itself to generate wavelength-dependent patterns (as in a grating demultiplexer) or resonances (as in a Fabry–Perot cavity), so that we can design optical devices with specific photon-absorbing spectrums based on these patterns or resonances. For this device, we use externally generated interference patterns so that we can take advantage of the relative position between the interference patterns and photodetector elements [metal–semiconductor–metal (MSM) devices] to generate specific spectral responses in the resulting photocurrent.

Specifically, in our new approach [1], we interfere a beam with a delayed version of itself to form an interference pattern on top of the multiple fingers of an MSM photodetector structure. The multiple fingers can be individually either positively

Manuscript received December 29, 2008; revised June 29, 2009 and August 24, 2009. First published September 18, 2009; current version published October 16, 2009. This work was supported in part by the Defense Advanced Research Projects Agency under the Chip-Scale Wavelength-Division Multiplexing Program through Army Research Office.

R. Chen was with the Solid State and Photonics Laboratory, Department of Electrical Engineering, Stanford University, Stanford, CA 94305 USA. He is now with Linear Technology Corporation, Milpitas, CA 95035 USA (e-mail: raychen@stanfordalumni.org).

J. Fu was with the Center for Integrated Systems, Stanford University, Stanford, CA 94305 USA. He is now with Exponent Failure Analysis Associates, Inc., Menlo Park, CA 94025 USA.

D. A. B. Miller is with the Solid State and Photonics Laboratory, Department of Electrical Engineering, Stanford University, Stanford, CA 94305 USA.

J. S. Harris, Jr. is with the Center for Integrated Systems, Stanford University, Stanford, CA 94305 USA.

Color versions of one or more of the figures in this paper are available online at http://http:ieeexplore.ieee.org.

Digital Object Identifier 10.1109/JLT.2009.2032248

or negatively biased to generate corresponding positive or negative photocurrent from the device. Then, we can choose an appropriate pattern of positive and negative biases of the MSM elements such that the net photocurrent collected is only from the desired wavelength, with cancelation of the current from the undesired wavelengths. Since the biasing pattern is simply a binary pattern of positive and negative voltages, the wavelength reconfiguration speed is essentially limited only by the electronic switching times of the bias pattern. We have already experimentally demonstrated a nanosecond wavelength reconfiguration time by flip-chip bonding the detector on a customized CMOS driver/receiver system [6]. In addition, we have also experimentally demonstrated that the spectral response of the detector can be shaped by using multiple different interference patterns to illuminate the device [7].

In this paper, we will theoretically describe how to design this CMOS-controlled tunable photodetector for multiple wavelength discrimination from our derived interference model in [1]. We will introduce two design algorithms for this device as design references: one is based on Fourier series, and the other is actually a very special and interesting case of the Fourier-series-based design algorithm converged in "SINC" form. Both of them share the same orthogonal basis, which will be described in Section II, for spectrum synthesis.

## II. Orthogonal Basis and Physical Devices

Our device design is based on a Fourier series technique, which will be explained well in Section III. In this section, we will discuss the relation of the mathematical orthogonal basis functions of the Fourier series and the device physical structures.

As we have mentioned in Section I, most of the wavelength-sensitive optical devices rely on interference of the signal wave in one form or another. The key to the operation of our device is the interference of a beam with a delayed version of itself on a multifingered detector. Fig. 1 is an example of a simplified Michelson interferometer unit as a standing wave generator. Other possible free-space interferometer configurations are discussed in [8]. In Fig. 1, the monochromatic tunable source beam enters from the bottom and splits into two parts at the 50/50 beam splitter into two paths of possibly different lengths. Then these two beams are interfered on the device through a converging lens. (In practical operation in networks, we would have a waveglength-division-multiplexed signal beam instead of the tunable monochromatic source.) The path length difference between the two interfering beams in Fig. 1 is $2|L_2 - L_1| = \Delta d$ and $\theta/2$ is the incident angle of the two interfering beams. This path length $\Delta d$ is a very important parameter to determine both how rapidly the interference pattern changes cyclically as we change the wavelength (what we will call the first harmonic repetition rate) and for aligning the spatial position (or spatial phase) of the interference pattern on the device to set the precise center wavelength of the desired response. Equivalently, we can think of the first harmonic repetition rate as corresponding to an effective free spectral range (FSR) of the device. The incident angle of the two interfering beams determines the spatial width of the fringe. In our application, the interference pattern landing area of the device has to be the same as the fringe width.

In the first-order approximation and as derived in [1], by ignoring the constant term, the interference pattern intensity

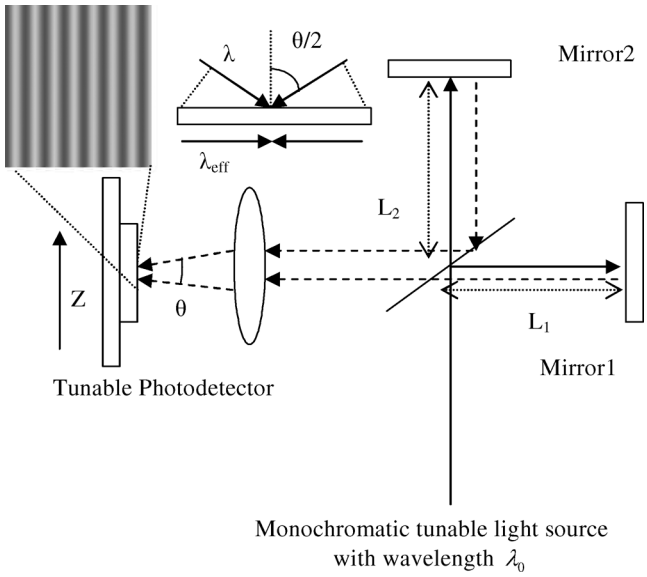


Fig. 1. Simplified Michelson interferometer as both the standing wave generator and the WDM channel spacing controller.

can be expressed as in (1), where $\lambda_0$ is the center wavelength of the signal (the monochromatic tunable wavelength in Fig. 1), $n$ is the refractive index of the medium, which is air in our prototype system, $k_{\text{int}} = 4\pi n \sin(\theta/2)/\lambda_0$ is the wave vector of the spatial interference pattern, $\beta(\Delta d) = 2\pi n \Delta d/\lambda_0$ is a constant phase term associated with $\Delta d$, and $\Phi(\lambda, \Delta d) = 2\pi n \Delta d(\lambda - \lambda_0)/\lambda_0^2$ is the phase term associated with both path length difference $\Delta d$ and any wavelength $\lambda$. The interference pattern intensity is actually always a positive number, but we always need to bias our device section under the illumination of the interference in a way that the averaging intensity term in the interference pattern is canceled out, which will also be explained later. Hence, for simplicity, we just ignore the constant term in our interference pattern formula in the following equation:

$$I(z, \lambda) \propto \cos(k_{\text{int}} z + \beta(\Delta d) - \Phi(\lambda, \Delta d)). \tag{1}$$

If $\lambda$ is exactly at $\lambda_0$ in (1), then the interference pattern intensity is in cosinusoidal along the $z$ axis as expected.

The basic device structure has $N$ fingers with half of them positively biased and half of them negatively biased, as always in our design. Since MSM photodetectors, shown in simplified versions in Fig. 2(a) and (b), have symmetrical physical structures, they should have symmetrical photocurrent response for positive and negative bias voltages, as shown in Fig. 2(c), if both the Bias electrode and the Gnd electrode are coated with the same type of metal. If the device is biased positively to the virtual ground node, photocurrent flows from the biasing node to the virtual ground node and *vice versa*. Hence, by referring to Fig. 3, any constant term in the interference pattern illuminating on the device will cause zero net photocurrent response out of the detector. That is why we can ignore the constant term in the intensity form and reduce it to be as in (1) for further mathematical analysis.

For simplicity, we take a two-fingered device, with one finger positively biased and the other negatively biased, as shown in

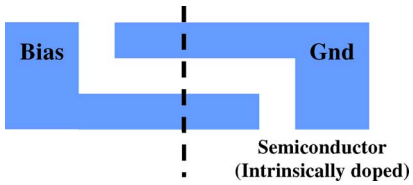


(a)

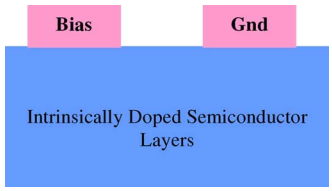


(b)

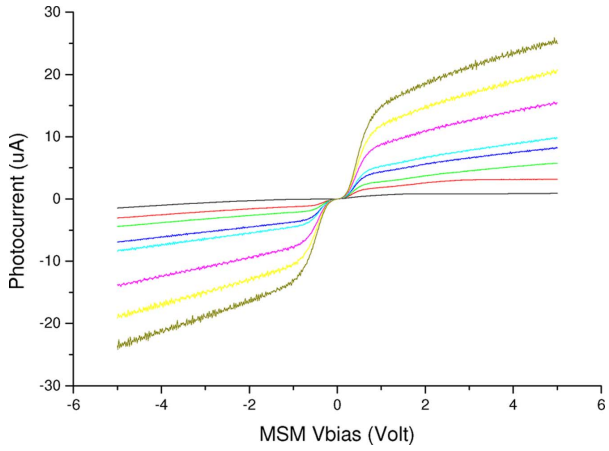


(c)

Fig. 2 (a) MSM photodetectors have symmetrical physical structures to cause symmetrical photocurrent response to CW beam with respect to 0 V across the two terminals. (b) Cross-section view of the MSM device in Fig. 2(a). If the Bias electrode and the Gnd electrode are coated with the same type of metal, the Schottky barriers between the Gnd node to the intrinsically doped semiconductor and the Bias node to the intrinsically doped semiconductor are exactly the same. (c) MSM photodetector, fabricated on InGaAs active layer with InGaAs/InAlAs barrier layer, has symmetrical photocurrent response under the illumination of 1550 nm CW beam with respect to 0 V across the two terminals. The different traces in the figure correspond to photocurrent responses with respect to different illuminating optical power intensity.

Fig. 3, to show that the device structure together with interference pattern shining on it can correspond to a basis function of a Fourier series.

For the device structure in Fig. 3, let us positively bias region I and negatively bias region II. First, we can choose $\Delta d$ such that $\beta(\Delta d) = -\pi/2$ in $I(z,\lambda)$, so that the interference pattern at the center wavelength $\lambda_0$ is shown as the dashed, blue sinusoidal shape in Fig. 3. With this choice, the photocurrent spectral response of this simple MSM structure is cosinusoidal in the wavelength domain with center wavelength $\lambda_0$ as in (2). We can alternatively choose $\Delta d$ such that $\beta(\Delta d) = 0$ in $I(z,\lambda)$, so that the interference pattern at the center wavelength $\lambda_0$ is shown as solid, red cosinusoidal shape in Fig. 2. With this choice, the

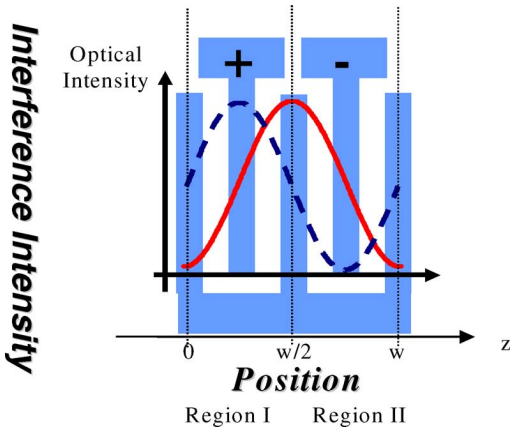


Fig. 3. Combination of both the solid interference pattern and the dashed interference pattern, and the MSM device basis with two biasing nodes forms the orthogonal basis of this tunable detector design.

photocurrent spectral response of this simple MSM structure is sinusoidal in the wavelength domain with center wavelength $\lambda_0$ as in (3). In the derivation of (2) and (3), $\mathrm{V_B}$ stands for the sign of the voltage that are applied to the biasing electrodes (i.e., here, $\mathrm{V_B}$ takes a value of either $+1$ or $-1$ corresponding to the bias polarity). We further assume that the width of the electrodes is infinitely small. In fact, if the finger spacing and width are identical, we will get the same mathematical format as (2) and (3). The only difference is the leading constant, which does not affect the validity of the rest of the derivation

$$\begin{aligned} I_{ph\_\cos}(\lambda) &\propto \int_{z=0}^{z=w} I(z,\lambda)|_{\beta(\Delta d)=-\pi/2}\mathrm{V_B}dz \\ &= \int_{z=0}^{z=w/2} \sin(k_{\mathrm{int}}z - \Phi(\lambda,\Delta d))dz \\ &\quad - \int_{z=w/2}^{z=w} \sin(k_{\mathrm{int}}z - \Phi(\lambda,\Delta d))dz \\ &\propto \cos(\Phi(\lambda,\Delta d)) = \cos\left(\frac{2\pi n\Delta d\,(\lambda-\lambda_0)}{\lambda_0^2}\right) \end{aligned} \tag{2}$$

$$\begin{aligned} I_{ph\_\sin}(\lambda) &\propto \int_{z=0}^{z=w} I(z,\lambda)|_{\beta(\Delta d)=0}\mathrm{V_B}dz \\ &= \int_{z=0}^{z=w/2} \cos(k_{\mathrm{int}}z - \Phi(\lambda,\Delta d))dz \\ &\quad - \int_{z=w/2}^{z=w} \cos(k_{\mathrm{int}}z - \Phi(\lambda,\Delta d))dz \\ &\propto \sin(\Phi(\lambda,\Delta d)) = \sin\left(\frac{2\pi n\Delta d\,(\lambda-\lambda_0)}{\lambda_0^2}\right). \end{aligned} \tag{3}$$

By observing the relative position between the interference pattern and the device biasing pattern in Fig. 3, we can see that the solid, red interference pattern is symmetric with respect to

the center line ($z = w/2$) of the device. Hence, in this case, the photocurrent response would be zero at the center wavelength $\lambda_0$. The dashed, blue interference pattern is antisymmetric with respect to the center line ($z = w/2$) of the device. Therefore, in this second case, the photocurrent response would be a maximum at the center wavelength $\lambda_0$. For $N$ wavelength discrimination, we will see in later sections of this paper that each basis device section needs to have at least $N$ fingers for this algorithm. For each specific wavelength selection, we bias the fingers in each basis device section as follows. Keeping the biasing pattern in phase with the interference pattern will generate a cosinusoidal harmonic spectral response as in (2). On the other hand, keeping $\pi/2$ phase shift between the biasing pattern and the interference pattern will generate a sinusoidal harmonic spectral response as in (3).

Note that, as a first-order approximation, we use the path length difference $\Delta d$ to determine both the repetition rate (period) of the spectral response with respect to wavelengths of the basis device structure and the relative phase of the spectral response with respect to wavelengths [the photocurrent format in either sinusoidal form or cosinusoidal form in (2) or (3)]. How do we use $\Delta d$ to determine two parameters, the period [$P_{\text{eriod}}$ in (4)], and the phase [$\beta(\Delta d)$] of the response? The answer is that we use the overall size of $\Delta d$ to set the period, and a very small adjustment, on a wavelength scale to set the phase. Let us illustrate this by substituting numerical values for both parameters, $P_{\text{eriod}}$ and $\beta(\Delta d)$. For $\lambda_0 = 1.55$ $\mu$m, let us take $P_{\text{eriod}} = 0.8$ nm (100 GHz in the C-band) as an example, which gives a value $\Delta d_o \sim 3$ mm in this case. Now, imagine that we make a small additional change $\delta d$ to set the phase, i.e., we write $\Delta d = \Delta d_o + \delta d$. From (4), the maximum amount of $\beta(\Delta d)$ change we need is $2\pi$

$$P_{\text{eriod}} = \left.\frac{\Phi(\lambda, \Delta d)\lambda_0^2}{2\pi n \Delta d}\right|_{\Phi(\lambda,\Delta d)=2\pi} = \frac{\lambda_0^2}{n\Delta d}. \tag{4}$$

As a result, we need to be able to have at most $\beta(\delta d) = 2\pi n \delta d/\lambda_0|_{\lambda_0=1.55\ \mu\text{m}} = 2\pi$, and hence, we only need a change $\delta d \sim 1.55$ $\mu$m. Therefore, the change required in $\Delta d$ to set the phase of the interference pattern is so small in practice that it makes negligible difference to the period of the spectral response.

By examining the numeric value $\Delta d$ in the earlier example, we can see that we should adjust $\Delta d$ in millimeters in free-space optics for FSR tuning and $\Delta d$ in micrometers in free-space optics for the relative phase between the interference pattern and the illuminated device. In practical setup in the laboratory, we use piezoelectric crystal to adjust $\Delta d$ in micrometers, and we move the whole reflecting mirror in one Michelson arm to adjust $\Delta d$ in millimeters.

From the earlier derivations (2) and (3), we can have either a cosinusoidal spectral response or a sinusoidal spectral response as our basis device structures. We could also construct additional interference patterns in different interferometers in which we choose $\Delta d$ to be integer multiples of the fundamental distance. In this way, we can construct a device basis for engineering spectral responses that go beyond a simple sinusoidal response with wavelength. In (2), if $\Delta d$ is doubled, the spectral response runs two times faster with respect to wavelengths. The corresponding device section, under the illumination of interference pattern with the path length difference $2\Delta d$ between the two interfering beams, has a second harmonic spectral response. In addition to this, we can use optical power intensity in the corresponding interference pattern to control the amplitude of the harmonic spectral response, assuming that the device is not saturated with photons. As a result, this simple device structure along with its specific interference pattern phase and period combination forms a complete orthogonal basis for Fourier-series-based spectral synthesis. We will discuss this multiple interferometer approach in Section III.

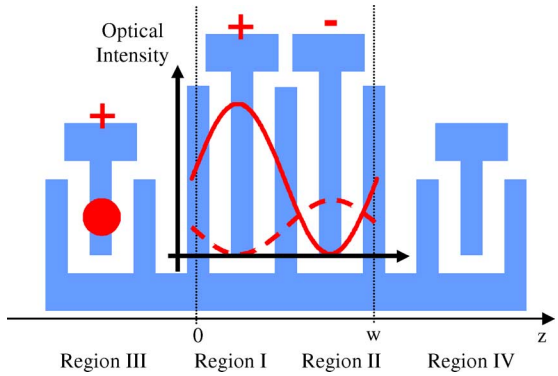


(a)

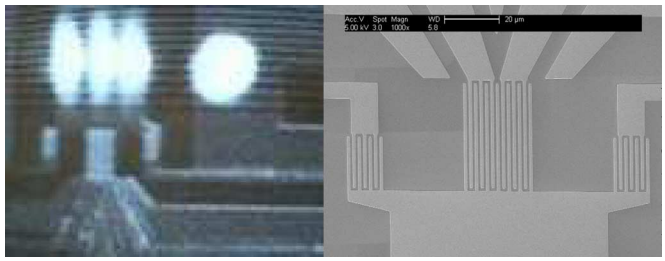

(b)

Fig. 4 (a) Synthesized device under the illumination of one solid interference pattern, one dashed interference pattern, and one CW beam for two wavelength discrimination. The device is a compact version of Fig. 6. (b) Fabricated device of Fig. 4(a) is shown in the right photograph and the device under illumination is in the left photograph, with an interference pattern on the left of the photograph and a CW beam on the right of the photograph. The specific interference pattern shown here is for the case of two overlapping interference patterns with different path length delays, as discussed in Section III.

If we take the basic device structure under the illumination of either interference pattern in Fig. 3 and add another continuous-wave (CW) beam such that the lowest output value is zero (rather than negative), we will get the measured spectral response in Fig. 5 and a curve fit from (5). The synthesized device consisting of the basic device structure under the illumination of only the solid interference pattern for now and a dc shift part is shown in Fig. 4(a). (Let us ignore the dashed interference pattern in Fig. 4(a) for now.) Fig. 4(b) shows the pictures of the fabricated device, and the device under the illumination of interference patterns and a CW beam.

Since this synthesized device has a sinusoidal spectral response with zero photocurrent minimum, this device can discriminate between wavelengths near a local maximum and a local zero minimum, as shown in Fig. 5. In terms of tuning, we

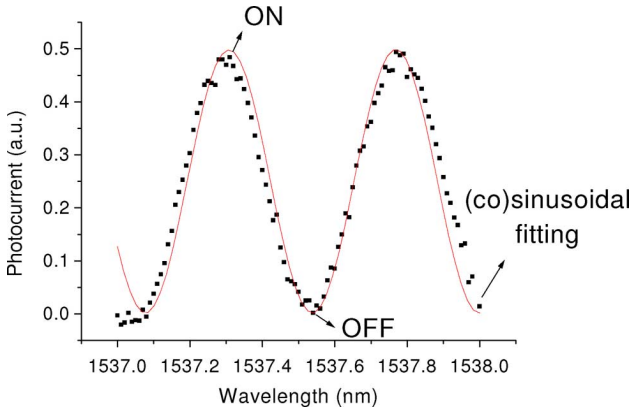


Fig. 5. Measured spectral response of the synthesized device under the illumination of only the solid interference pattern in Fig. 4. The synthesized device with this spectral response can discriminate between 1537.31 and 1537.54 nm band.

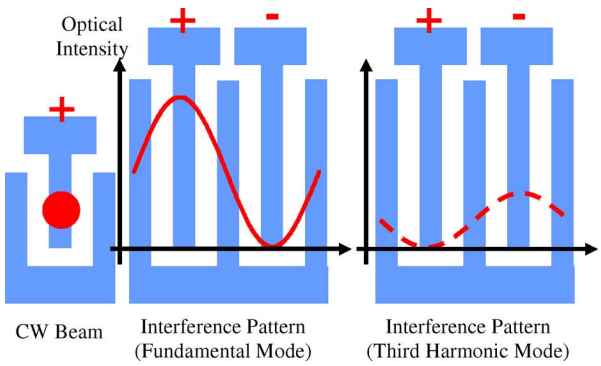


Fig. 6. Constructing the tunable detector with spectral response expressed in (9) based on basis structure in Fig. 3.

just need to swap the biasing between regions I and II, and we can get a totally complementary spectral response. Since we can change the spectral response by just changing the biasing pattern applied on the device, the switching speed of the device response is limited by the switching electronics, which is in the nanosecond range. The channel spacing in this measured device system is ~0.23 nm and the path length difference between the two interfering beams is ~5.138 mm. The device wafer structure and the measurement detail are clearly described in [7]

$$I_{2\lambda}(\lambda) = 0.24826 \left[1.007 + \cos\left(\frac{(\lambda - 1537.307)}{0.46088} 2\pi\right)\right]. \quad (5)$$

## III. Fourier-Series-Based Device Design

From the previous section and Fig. 3, we know that the relative phase shift between the interference patterns from a monochromatic source and the device biasing pattern determines the phase of the periodic spectral response. For a fixed device structure and biasing pattern, we can adjust the path length difference $\Delta d$ to achieve all of the harmonic functions in the orthogonal basis of Fourier series. In this section, we will describe how to combine the basis device structures to construct a photodetector with synthesized spectral response, allowing a spectral response that goes beyond a simple sinusoidal form.

From Fourier series theory, any periodic spectral response centered at center wavelength $\lambda_0$ in the wavelength domain can be expressed as superposition of a dc term, a fundamental term, and all of the harmonics as shown in (6), where $k_0 = 2\pi/P_{\text{eriod}}$, with $P_{\text{eriod}}$ being the period of the spectral response in the wavelength domain, and $a_m$ and $b_m$ can be expressed as in (7) and (8), respectively, when $m \geq 1$

$$S(\lambda) = c_0 + \sum_{m=1}^{\infty} a_m \cos(mk_0(\lambda - \lambda_0)) + \sum_{m=1}^{\infty} b_m \sin(mk_0(\lambda - \lambda_0)) \quad (6)$$

$$a_m = \frac{2}{P_{\text{eriod}}} \int_{\langle P_{\text{eriod}} \rangle} S(\lambda) \cos(mk_0(\lambda - \lambda_0)) d\lambda \quad (7)$$

$$b_m = \frac{2}{P_{\text{eriod}}} \int_{\langle P_{\text{eriod}} \rangle} S(\lambda) \sin(mk_0(\lambda - \lambda_0)) d\lambda. \quad (8)$$

As a result, for any desired photocurrent spectral response, we can use multiple copies of the structure in Fig. 3, along with appropriate corresponding interference pattern phases, amplitudes, and repetition rates in the wavelength domain and synthesize it.

If $S(\lambda)$, the targeted detector spectral response, is an even function with respect to the laser carrier wavelength $\lambda_0$ from the transmitter side, which is usual for spectral responses of most of the optical filters, $b_m$ is equal to zero. Under this circumstance, we just need the basis device biasing patterns in phase with its corresponding interference pattern, like the dashed blue one in Fig. 3, for any harmonics of the fundamental spectral response. However, based on this design methodology, unlike other types of optical filters, the spectral response of the detector does not have to be symmetrical with respect to the laser carrier wavelength for maybe some specific signal processing purpose. In fact, only half of the spectrum information is enough to recover the whole baseband information. For this case, we need to use the device structure with both interference pattern phases in Fig. 3 to synthesize the desired photocurrent spectral response.

Let us take two examples illustrating how to use the basis device structure along with the corresponding interference patterns to design detectors with desired spectral response. The first example is to use two interference patterns with different path length differences $\Delta d$ to synthesize a spectral response with relatively flat passband and stopband for two wavelength discrimination. The goal of this design is to make the detector almost square in its amplitude response, approximating a repeating square response with 50% duty cycle. If we decompose this "spectral response" into its fundamental mode and the superposition of all harmonics, we will get the following equation if we truncate all of the higher order terms:

$$I_{ph\_2\lambda} \propto \left(0.785 + \cos\left(\frac{2\pi n \Delta d(\lambda - \lambda_0)}{\lambda_0^2}\right) - \frac{1}{3}\cos\left(3\frac{2\pi n \Delta d(\lambda - \lambda_0)}{\lambda_0^2}\right)\right). \quad (9)$$

For the spectral response in (9), we have two cosine terms: one is the third harmonic of the other and the other is the DC

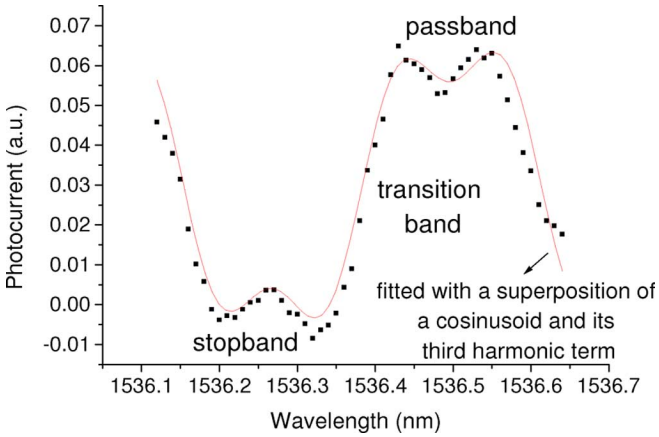


Fig. 7. Measured spectral response of device structure under the illumination of two interference patterns in Fig. 4(a).

term. Since there are two cosine terms in (9), we know that we should use two copies of the basis device structure along with the blue, dashed interference pattern in Fig. 3 and one DC term to implement the detector, as shown in Fig. 6. The second copy of the basis device should be illuminated from an interferometer with three times as large a path length difference. Note that the negative sign in front of the third harmonic cosine term corresponds to a $\pi$ phase shift with respect to the dashed, blue interference pattern for the basis device structure in Fig. 3. The ratio of the dc value and the coefficients in front of the cosine terms in absolute value corresponds to the relative interference power intensity among the CW beam, the first harmonic interference, and the third harmonic interference. In Fig. 6, by combining the two basis device structures together, we can get a compact device under the illumination of two interference patterns in Fig. 4(a). Now, we should look at both the solid and the dashed interference patterns landing on the device in Fig. 4(a). Fig. 4(b) shows the fabricated device, the device under the illumination of two interference patterns, and one CW beam in the experiments. The measured synthesized spectral response, curve fitted to (10), is shown as the dotted line in Fig. 7

$$I_{2\lambda}(\lambda) = 0.03592 \begin{bmatrix} 0.835 + \cos\left(\frac{(\lambda - 1536.499)}{0.45911} 2\pi\right) \\ -0.2784 \cos\left(\frac{(\lambda - 1536.499)}{0.45911} 3 \times 2\pi + 0.1\right) \end{bmatrix}. \quad (10)$$

In this experiment, the path length difference between the two interfering beams of the first interference pattern is ~5.138 mm and the path length difference between the two interfering beams of the second interference pattern is ~15.413 mm. In (10), the detector can now discriminate not only between 1536.27 and 1536.50 nm with 0.23 nm channel spacing, but also discriminate between signals in its relatively flat passband and those in its similarly flat stopband. Comparing (9) and (10), the experimental result matches the theoretical design relatively well, although with 0.1 rad phase skew. The experiment and wafer structure detail is described in [7].

As for the tunability of the device in Fig. 4(a), we just need to swap the biasing polarity between region I and region II to reconfigure the spectral response, changing the passband to the stopband and *vice versa*.

The second example is to use one fundamental term and its second harmonic to design a detector discriminating four wavelengths. In this example, the "space-to-mark ratio" of its ideal spectral response determines the Fourier coefficients among the dc and harmonics terms. In our example, we choose the space-to-mark ratio to be three—i.e., ideally, the detector would detect wavelengths within one "square" spectral band and reject within an adjacent band three times wider. The Fourier analysis of such a spectral band response is analogous to that of square pulses with 25% duty cycle, and the targeted synthesized spectral response is shown in (11). We get (11) by decomposing a periodic pulse "train" with 25% duty cycle in the wavelength domain into the fundamental term and a superposition of all of the harmonics, and then truncate those harmonic terms higher than the second

$$I_{ph\_4\lambda} \propto \left(\frac{\pi}{2} + \sqrt{2}\cos\left(\frac{2\pi n \Delta d(\lambda - \lambda_0)}{\lambda_0^2}\right) + \cos\left(2\frac{2\pi n \Delta d(\lambda - \lambda_0)}{\lambda_0^2}\right)\right). \quad (11)$$

The device implementation is illustrated in Fig. 8(a). The device in Fig. 8(a) has three sections corresponding to the DC section, Section I for the fundamental term, and Section II for the second harmonic term. Since we have only cosine terms in (11), we just need to apply the biasing pattern in phase with the interference pattern for both Sections I and II. This is like the relative device biasing and blue dashed interference pattern relation in Fig. 3. The simulated spectral response for this biasing state is shown as the thicker, darker trace in Fig. 9.

## IV. Device Tuning

So far we have described how to design an optical detector with a filtering spectral response, but have not described how to choose the biasing patterns applied on those device sections for different wavelength selection. In this section, we will describe how to choose these biasing patterns. The tuning algorithm we describe here assumes the use of the minimum number of biasing fingers per MSM harmonic section.

Let us take four-wavelength discrimination devices, with designed spectral response as shown in (11), as an example. It is quite illustrative to use the "constellation diagram" in Fig. 10 to describe this biasing algorithm. In Fig. 10, the *x* axis stands for the wavelength $\lambda$ and the *y* axis stands for the "relative" interference pattern phase shift with respect to wavelength $\lambda_0$, as shown in the following equation and derived in [1]:

$$\Phi(\lambda, \Delta d) = 2\pi n \Delta d/\lambda_0^2 \cdot (\lambda - \lambda_0). \quad (12)$$

In Fig. 10, the solid line with slope $2\pi n \Delta d/\lambda_0^2$ represents the relative interference pattern phase shift with respect to $\lambda_0$ for the first harmonic (fundamental term) MSM device section and the dashed line with slope $2\pi n(2\Delta d)/\lambda_0^2$ represents the relative interference pattern phase shift with respect to $\lambda_0$ for the second harmonic MSM device section. For design simplicity concern, let us choose the finger width of each MSM absorption region to be identical. In other words, the semiconductor absorption area corresponding to each finger is the same.

The goal of this device design is to use two MSM harmonic sections to synthesize the spectral response of the detector to

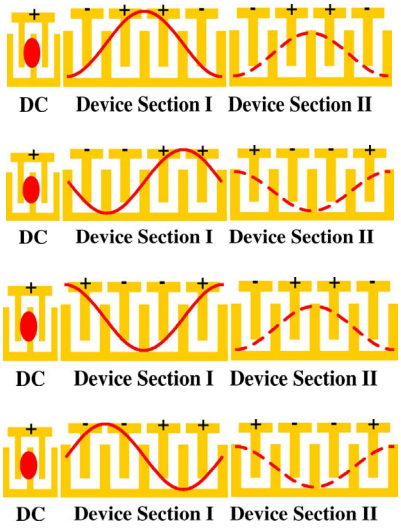


Fig. 8 (a) There are three sections, the DC section, and Sections I and II, in this four-wavelength discrimination device. The interference pattern landing on the device in Section II runs two times faster than that landing on the device in Section I with respect to the wavelength. The photocurrent spectral response in Section II is the second harmonic with respect to wavelength of the spectral response in Section I. The device biasing pattern shown here is used to select the first channel. (b) This device biasing pattern is used to select the second channel. The biasing pattern changes in phase with the interference pattern. Comparing the phase shift between the interference patterns landing on the device for this state and the state in Fig. 8(a), there is a $\pi/2$ phase shift for the interference pattern landing on the device in Section I and there is a $\pi$ phase shift for the interference pattern landing on device in Section II. (c) This device biasing pattern is used to select the third channel. The biasing pattern changes in phase with the interference pattern. (d) This device biasing pattern is used to select the fourth channel. The biasing pattern changes in phase with the interference pattern.

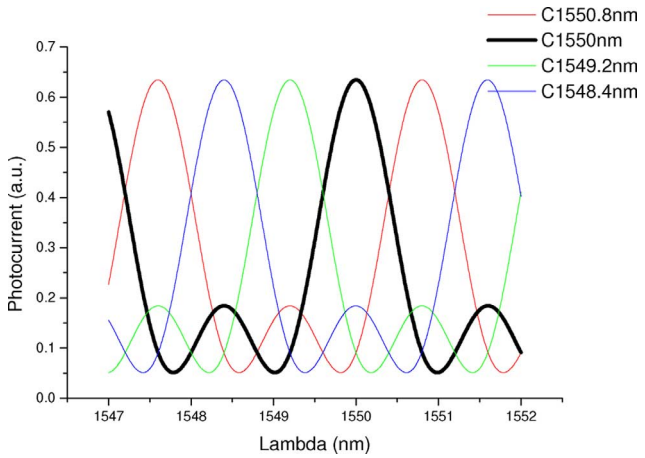


Fig. 9. Simulated spectral responses for this four-wavelength discrimination device in the Fourier-series-based algorithm. The spectral response with a center wavelength of 1550 nm is highlighted as the thicker trace.

be (11) for four wavelength discrimination. The easiest way is to evenly distribute the four phases in the $2\pi$ period cycle for the first harmonic section (the fundamental term section). (It is not absolutely necessary to evenly distribute the four phases in the $2\pi$ period cycle, but uneven distributions of phase will lead to more MSM fingers per section.) Therefore, there are four equally distributed constellation points, four solid dots, on the solid line in Fig. 10. Since we have four evenly distributed constellation points in the solid line in Fig. 10, we have four discrete

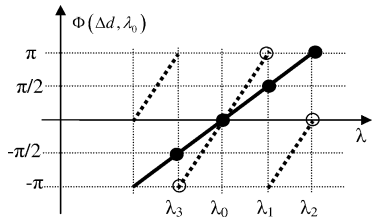


Fig. 10. Constellation diagrams showing four discrete states of this four-wavelength discrimination device. The $y$ axis stands for the interference relative phase shift of each discrete state with respect to the $\lambda_0$ state. The $x$ axis stands for the wavelength. The solid dots correspond to the phase of the interference pattern of Section I, and the hollow dots correspond to that of Section II. At the $\lambda_0$ state, the solid dot and the hollow dot overlap with each other.

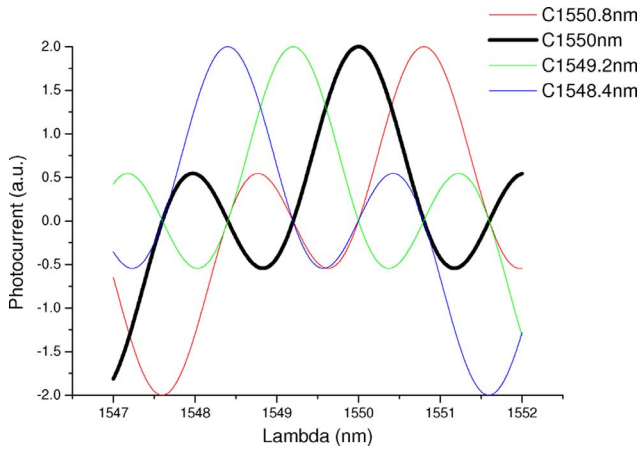


Fig. 11. Simulated spectral responses of the four-wavelength discrimination device in a SINC-based algorithm. The spectral response with center wavelength at 1550 nm is highlighted as the thicker trace.

phase states for the biasing pattern for the first device section. As a result, we need to have at least four fingers for each section of the four-wavelength discrimination device. Note that this applies if we would like to evenly distribute any number of constellation points within a $2\pi$ period cycle. Accordingly, the biasing pattern applied on it should shift cyclically to the right for one finger out of the total four fingers as the input wavelength is switched to the adjacent channel.

The same biasing principle applies to the device section for the second harmonic, except that the phase shift between each adjacent constellation points is doubled for the second harmonic case (tripled for the third harmonic case, etc.) compared to the fundamental one. This is because the interference pattern runs two times faster compared to the fundamental one as the wavelength is tuned. Therefore, the phase shift between the two adjacent constellation points (the hollow dots) in the second harmonic mode line (the dashed line) in Fig. 11 has to be $\pi$. Applying the same principle as we explained in Section I, we should cyclically shift the biasing pattern to the right for two fingers in Section II. Note that at state $\lambda_0$, the solid dot overlaps with the hollow dot in Fig. 10.

In fact, for each channel wavelength in the constellation diagram in Fig. 10, the vertical line we draw from the wavelength axis should pass two constellation dots, corresponding to the fundamental and the second harmonic terms. Fig. 8(a)–(d) shows the biasing pattern of the four-wavelength discrimination

device for each harmonic section. They also show the four interference pattern states corresponding to the four device biasing patterns for four different channels.

By applying the same method to the device we have analyzed in Fig. 4(a), it is very straightforward to understand that we just need to toggle the two fingers in regions I and II of the device in Fig. 4 to select the two channels with channel spectral response shown in Fig. 7.

From the device tuning algorithm described in this section, we can see that for a $N$ wavelength discrimination device, we need at least $N$ fingers per MSM device harmonic section and at least around $\log_2 N$ harmonic sections.

## V. Device Design Flow

In this section, we will summarize the device design flow for the Fourier-series-based design algorithm.

1) Specify the spectral response for a single channel of the device that meets the system requirement. Remember that this spectral response has to be periodic although the spectral response can be designed such that the period of the response is longer than the band of interest.
2) Decompose the desired detector spectral response based on Fourier series by using (6)–(8). In this step, the number of harmonic device sections and the number of channels to be discriminated should be determined.
3) Draw the figure for the device under design like Fig. 6 or Fig. 8(a) based on Fig. 3.
4) Draw the constellation diagram like Fig. 10 to pattern the MSM biasing patterns for each channel (wavelength) and get a figure like Fig. 8(a)–(d).
5) These MSM biasing pattern in "binary format" can be regarded as a logic state, and standard logic finite-state machine technique can be used to design CMOS drivers to set these states based on system needs.

## VI. Sinc-Function-Based Designs

The Fourier-series-based design described before is an approximation to the ideal spectral response, and we think this Fourier-series-based design can be practically used to meet all kinds of system requirements as long as more harmonics (interference patterns) can be incorporated at the cost of increased system complexity. In the Fourier-series-based design, we do not design the spectral response of the detector to exactly nullify some specific wavelengths. Instead, we specify the ripple amplitude in both passband and stopband, and the sharpness of the transition band. Another interesting method for designing this device is to nullify the exact center wavelength of the adjacent channels, which will be described in this section. The disadvantage of this design method is that the slopes of the detector spectral response at the nullified wavelengths are relatively sharp so that the response is sensitive to any wavelength variation or modulation. However, it could be useful in some specific sensing systems. Interestingly enough, the analytical form of this design for discriminating wavelengths at a large number will mathematically converge to a "sinc" function, which will be derived later in this section.

In this design, we just need to use a subset of the orthogonal functions in the orthogonal basis, which are "cosine" based orthogonal functions in odd order as in (2). Hence, in physical implementation, we just need to use the basis device structure illuminated with interference patterns like the blue dashed in Fig. 3.

Before deriving the mathematical results, we first note some trigonometric identities. First, $\cos(\pi/4)+\cos(3\pi/4)=0, \cos(2\pi/4)+\cos(6\pi/4)=0$, and $\cos(3\pi/4)+\cos(9\pi/4)=0$. Second, $\cos(0)+\cos(0)=2$. Based on these identities, we can see that the spectral response, as shown in (13), will give a four-wavelength discrimination device, i.e., a device that responds to one wavelength but has exactly no response at another three (equally spaced) wavelengths

$$I_{ph\_4\lambda\_\sin c} \propto \left(\cos\left(\frac{2\pi n\Delta d(\lambda-\lambda_0)}{\lambda_0^2}\right) + \cos\left(3\frac{2\pi n\Delta d(\lambda-\lambda_0)}{\lambda_0^2}\right)\right). \quad (13)$$

Equation (13) can be plotted as the thick trace shown in Fig. 11 for $\Delta d = 0.3754$ mm and $\lambda_0 = 1550$ nm. The physical meaning of the earlier equation is that we have two MSM device sections under the illumination of two interference patterns, respectively. The second interference pattern shining on the second MSM device section moves three times faster with respect to the wavelength than that of the first pattern shining on the first MSM device section. The photocurrent spectral response of the second MSM device section is the third harmonic of that of the first one. This newly synthesized device, with spectral response traces for four different biasing states as shown in Fig. 11, can discriminate four wavelengths. Only one wavelength is activated at a time. On wavelength tuning, the biasing finger pattern applied on the device follows the same guideline as that for the Fourier-series-based algorithm. We always positively bias the device sections under the illumination of positive part of the interference pattern of (13) and negatively bias the device sections under the illumination of negative part of the interference pattern of (13). For the device designed for four wavelength discrimination with the spectral response shown in Fig. 11, we consequently need eight fingers per device section because there are eight different possible regions of positive or negative sign of interference, each spaced by $2\pi/8$ rad of phase difference. Note that only four fingers per device section are needed for the Fourier-series-based algorithm, as described in Sections IV and V.

Another even simpler example is to design a two-wavelength discrimination device. Again, let us observe the following trigonometry relation: $\cos(\pi/2)=0$ and $\cos(0)=1$. The physical meaning of the aforementioned math equations is that we need only one two-fingered device section with one interference pattern shining on it for two wavelength discrimination. This device can discriminate between two wavelengths corresponding to two phases of an interference pattern. The phase shift between the two phases is $\pi/2$. A third example is the design of a device that can discriminate among eight wavelengths.

From $\cos(\pi/8)+\cos(3\pi/8)+\cos(5\pi/8)+\cos(7\pi/8)=0$, it can be deduced that this device with four MSM sections can discriminate eight wavelengths based on the same principle as that for the four-wavelength discrimination device. As a conclusion from induction, if we would like to discriminate between $2^N$

wavelengths in this device, we need to have $2^{N-1}$ device sections and $2^{N-1}$ harmonic spectral responses with the same amplitude all added together. The first harmonic interference pattern phase difference between adjacent channels is $2\pi/2^{N+1}$. The overall photocurrent spectral response is derived in (14) according to the basis from (2), where we replace $\lambda-\lambda_0$ in the derivation by $\Delta\lambda, 2\pi n\Delta d/\lambda_0^2$ by $k_0$, and $2^{N-1}-1$ by $M$.

The photocurrent convergence form derived in (14) so far has no approximation at all. If we would like the generic derivation in (14) to be converged into an even more succinct form, we need to impose one more constraint in (14) to link up $k_0$ and $2^N$. The constraint imposed on (14) is that we want the channel spacing or FSR between two adjacent wavelengths to be fixed as the number of wavelengths approaches $2^N$. Since we want the device to discriminate $2^N$ wavelengths, we want the interference pattern phase difference between two adjacent wavelengths to be $\Phi(\lambda,\Delta d)=2\pi/2^{N+1}$, as we deducted before. From $\Phi(\lambda,\Delta d)=2\pi n\Delta d(\lambda-\lambda_0)/\lambda_0^2$, we can set up the FSR, $\mathrm{FSR}=\lambda-\lambda_0$, in (15). By substituting from (15) into $k_0=2\pi n\Delta d/\lambda_0^2$, we will get (16)

$$\begin{aligned}
I_{\mathrm{ph}}(\lambda) &= \sum_{i=0}^{2^{N-1}-1}\cos[k_0(2i+1)(\lambda-\lambda_0)] \\
&= \sum_{i=0}^{M}\cos[k_0(2i+1)\Delta\lambda] \\
&= \frac{1}{2}\sum_{i=0}^{M}[\exp(jk_0(2i+1)\Delta\lambda) \\
&\quad +\exp(-jk_0(2i+1)\Delta\lambda)] \\
&= \frac{1}{2}\sum_{i=0}^{M}[\exp(jk_0\Delta\lambda)+\exp(j3k_0\Delta\lambda) \\
&\quad +\exp(j5k_0\cdot\Delta\lambda)+\cdots] \\
&\quad +\frac{1}{2}\sum_{i=0}^{M}[\exp(-jk_0\Delta\lambda) \\
&\quad +\exp(-j3k_0\Delta\lambda) \\
&\quad +\exp(-j5k_0\Delta\lambda)+\cdots] \\
&= \frac{1}{2}\exp(jk_0\Delta\lambda)\frac{1-\exp(j2Mk_0\Delta\lambda)}{1-\exp(j2k_0\Delta\lambda)} \\
&\quad +\frac{1}{2}\exp(-jk_0\Delta\lambda)\frac{1-\exp(-j2Mk_0\Delta\lambda)}{1-\exp(-j2k_0\Delta\lambda)} \\
&= \frac{[\exp(jk_0\Delta\lambda)-\exp(-jk_0\Delta\lambda)]}{2[2-\exp(j2k_0\Delta\lambda)-\exp(-j2k_0\Delta\lambda)]} \\
&\quad [\exp(-j2Mk_0\Delta\lambda)-\exp(j2Mk_0\Delta\lambda)] \\
&= \frac{\sin(k_0\Delta\lambda)}{[1-\cos(2k_0\Delta\lambda)]}\sin(2k_0M\Delta\lambda) \\
&= \frac{\sin(2k_0M\Delta\lambda)}{2\sin(k_0\Delta\lambda)} = \frac{\sin(k_0(2^N-2)\Delta\lambda)}{2\sin(k_0\Delta\lambda)}
\end{aligned} \tag{14}$$

$$\mathrm{FSR}=\left.\frac{\Phi(\lambda,\Delta d)\lambda_0^2}{2\pi n\Delta d}\right|_{\Phi(\lambda,\Delta d)=\frac{2\pi}{2^{N+1}}}=\frac{\lambda_0^2}{2^{N+1}n\Delta d} \tag{15}$$

$$k_0=\frac{2\pi n\Delta d}{\lambda_0^2}=\frac{2\pi}{\mathrm{FSR}2^{N+1}}. \tag{16}$$

TABLE I
COMPARISON BETWEEN THE TWO DEVICE DESIGN ALGORITHMS

| | Number of wavelength discrimination | Number of MSM sections ( at least) | First Harmonic Phase Diff Between channels | Biasing fingers per section |
|---|---|---|---|---|
| Fourier Based Design | $N$ | $\sim \log_2 N$ | $2\pi/N$ | $N$ |
| "SINC" Based Design | $2^N$ | $2^{N-1}$ | $2\pi/2^{N+1}$ | $2^{N+1}$ |

By substituting (16) into (14), we will get (17) under the approximation of $\sin\theta\sim\theta$ when $N$ is a very large number

$$\begin{aligned}
I_{\mathrm{ph}}(\lambda) &= \frac{\sin\left(2\pi\frac{1}{\mathrm{FSR}}\left(\frac{2^N-2}{2^{N+1}}\right)\Delta\lambda\right)}{2\sin\left(2\pi\frac{1}{\mathrm{FSR}2^{N+1}}\Delta\lambda\right)} \\
&\sim \frac{\sin\left(\pi\frac{1}{\mathrm{FSR}}\Delta\lambda\right)}{2\pi\frac{1}{\mathrm{FSR}\cdot 2^N}\Delta\lambda}=2^{N-1}\frac{\sin\left(\pi\frac{\Delta\lambda}{\mathrm{FSR}}\right)}{\pi\frac{\Delta\lambda}{\mathrm{FSR}}} \\
&= 2^{N-1}\sin c\left(\pi\frac{\Delta\lambda}{\mathrm{FSR}}\right).
\end{aligned} \tag{17}$$

From the convergence form in (17), we can see that the main peak of the spectral response is the wavelength we would like to activate, and all of the other nulls in the "sinc" are exactly the wavelengths we would like to suppress.

The principle of physical device finger biasing is the same as the Fourier-series-based device design. In this device design, if we would like to discriminate $2^N$ wavelengths, we need to have at least $2^{N-1}$ device sections/interference harmonics and $2^{N+1}$ biasing fingers per device section. This device biasing algorithm might not work well for high-data-rate telecommunication applications because the ripples of the "sinc" function can cause severe crosstalk from the adjacent channels. However, since this design can exactly desensitize to the center carrier wavelength, it could be possibly useful for some sensing applications where we want to suppress the detection of the exciting wavelength, for example.

The comparison between the Fourier-series-based design algorithm and this "sinc" based design algorithm is concluded in Table I.

## VII. CONCLUSION

In this paper, we introduced and fully analyzed two possible design algorithms for this novel class of CMOS-controlled MSM-based tunable photodetectors. The first one is the Fourier-series-based algorithm, which can be used to synthesize any desired spectral responses, even responses not symmetrical with respect to the center laser carrier wavelength. Through this Fourier-series-based algorithm, the spectral response can be synthesized to be relative flat in both the passband/stopband and sharp in transition band, as would be required in telecommunication application. The other algorithm is the "sinc" function based algorithm. In this algorithm, the spectral response converges to a "sinc" form as the number of detector sections and interference patterns is large. This "sinc" based algorithm allows one wavelength to be activated

while exactly nullifying all of the other equally spaced channel wavelengths. This could be useful for sensing applications.

The tuning mechanism of this detector is by electrically changing the binary/digital biasing patterns applied on the devices to select among the WDM channels. The wavelength/channel reconfiguration time could therefore be much shorter (nanosecond scale) than the data packet length in telecommunication applications. Additionally, this wavelength reconfiguring process is relatively robust because the biasing pattern consists of a few binary digits, and this biasing pattern control circuit can be easily implemented through CMOS finite-state machine logic.

Component integration into one chip is critical for reducing system cost and facilitating system integration, which is one of the advantages we propose for this device. This paper merely demonstrates the feasibility of the novel detecting scheme in a proof of principle. In practical implementation, this apparatus design should ultimately be monolithically integrated with the detectors in order to form an integrated tunable detector or demultiplexing module.

## REFERENCES


[1] R. Chen, D. A. B. Miller, K. Ma, and J. S. Harris Jr., "Novel electrically controlled rapidly wavelength selective photodetection using MSMs," *IEEE J. Sel. Topics Quantum Electron.*, vol. 11, no. 1, pp. 184–189, Jan./Feb. 2005.

[2] K. W. Cheung, "Acoustooptic tunable filters in narrowband WDM networks: System issues and network applications," *IEEE J. Sel. Areas Commun.*, vol. 8, no. 6, pp. 1015–1025, Aug. 1990.

[3] K. Yu and O. Solgaard, "Tunable optical transversal filters based on a Gires–Tournois interferometer with MEMS phase shifters," *IEEE J. Sel. Topics Quantum Electron.*, vol. 10, no. 3, pp. 588–597, May/Jun. 2004.

[4] T. Amano, F. Koyama, T. Hino, M. Arai, and A. Mastutani, "Design and fabrication of GaAs-GaAlAs micromachined tunable filter with thermal strain control," *J. Lightw. Technol.*, vol. 21, no. 3, pp. 596–601, Mar. 2003.

[5] K. Lai and J. C. Campbell, "Design of a tunable GaAs/AlGaAs multiple-quantum-well resonant-cavity photodetector," *IEEE J. Quantum Electron.*, vol. 30, no. 1, pp. 108–114, Jan. 1994.

[6] R. Chen, H. Chin, D. A. B. Miller, K. Ma, and J. S. Harris, Jr., "MSM-based integrated CMOS wavelength tunable optical receiver," *IEEE Photon. Technol. Lett.*, vol. 17, no. 6, pp. 1271–1273, Jun. 2005.

[7] R. Chen, J. Fu, D. A. B. Miller, and J. S. Harris Jr., "Spectral shaping of electrically controlled MSM-based tunable photodetectors," *IEEE Photon. Technol. Lett.*, vol. 17, no. 10, pp. 2158–2160, Oct. 2005.

[8] D. A. B. Miller, "Lasers tuners and wavelength-selective detectors based on absorbers in standing waves," *IEEE J. Quantum Electron.*, vol. 30, no. 3, pp. 732–749, Mar. 1994.


**Ray Chen** (S'01–M'06) received the B.Sc. degree in electronics engineering from the National Chiao Tung University, Hsin-Chu, Taiwan, in 1997, and the M.S. and Ph.D. degrees in electrical engineering from Stanford University, Stanford, CA, in 2001 and 2006, respectively. His doctoral dissertation work was on CMOS-controlled rapidly tunable photodetectors under the supervision of Professor David A. B. Miller at Stanford.

From 1997 to 1999, he was with the Chinese Army as a Communication Technical Officer. During the summer of 2000, he interned at IBM Microelectronics, Essex Junction, VT, where he was working on in IC testing methodology for application-specific ICs. Since 2006, he has been with Linear Technology Corporation, Milpitas, CA, where he is engaged in designing high-speed pipeline-flash analog-to-digital converters.

Dr. Chen was one of the recipients of the 2005 IEEE Lasers and Electro-Optics Society Graduate Student Fellowship Award.

**Junxian Fu** (S'05–M'05) was born in Henan, China, in 1975. He received the B.S. and Ph.D. degrees in electronics from Beijing University, Beijing, China, in 1997 and 2000, respectively, and the M.S. degree in electrical engineering and the Ph.D. degree in applied physics from Stanford University, Stanford, CA, in 2003 and 2005, respectively.

He was involved in design, modeling, and fabrication of compact Fourier-transform spectrometer with novel optoelectronic devices. Since 2005, he has been with Exponent Failure Analysis Associates, Inc., Menlo Park, CA. His current research interests include failure analysis of microelectronic and optoelectronic systems and devices.

**David A. B. Miller** (M'84–SM'89–F'95) received the B.Sc. degree from St Andrews University, St Andrews, U.K., and the Ph.D. degree from Heriot-Watt University, Edinburgh, in 1979.

From 1981 to 1996, he was with Bell Laboratories, where he was a Department Head from 1987, and latterly of the Advanced Photonics Research Department. He is currently the W. M. Keck Professor of electrical engineering at Stanford University, Stanford, CA, where he is the Director of the Ginzton and Solid State and Photonics Laboratories. His research interests include quantum-well optoelectronic and nanophotonic physics and devices, and fundamental and applications of optics in information, sensing, switching, and processing. He is the author or coauthor of more than 200 scientific papers. He holds more than 55 patents.

Dr. Miller is a Fellow of the Royal Societies of London and Edinburgh, the Optical Society of America (OSA), and the American Physical Society. He was a Board member for both the OSA and the IEEE Lasers and Electro-Optics Society (LEOS), and also in various other society and conference committees. During 1995, he was the President of the IEEE LEOS. He was the recipient of the Adolph Lomb Medal and the R. W. Wood Prize from the OSA, the International Prize in Optics from the International Commission for Optics, and the IEEE Third Millennium Medal. He holds honorary degree from Vrije Universiteit Brussel and Heriot-Watt University.

**James S. Harris, Jr.** (S'65–M'69–SM'78–F'88) received the B.S., M.S., and Ph.D. degrees in electrical engineering from Stanford University, Stanford, CA, in 1964, 1965, and 1969, respectively.

In 1969, he joined Rockwell International Science Center, Thousand Oaks, CA, where he was one of the key contributors to ion implantation, molecular beam epitaxy, and heterojunction devices, leading to their preeminent position in GaAs technology. In 1980, he became the Director of the Optoelectronics Research Department. In 1982, he joined the Solid State Electronics Laboratory, Stanford University, as a Professor of Electrical Engineering, where he was the Director of the Solid State Electronics Laboratory (1984–98), the Director of the Joint Services Electronics Program (1985–99), and is currently the James and Ellenor Chesebrough Professor of Electrical Engineering, Applied Physics, and Materials Science in the Center for Integrated Systems. His research interests include physics and application of ultra-small structures and novel materials to new high-speed and spin-based electronic, and optoelectronic devices and systems. He is the author or coauthor of more than 650 publications. He holds 14 issued U.S. patents.

Dr. Harris is a Fellow of the American Physical Society. He was the recipient of the 2000 IEEE Morris N. Liebmann Memorial Award, the 2000 International Compound Semiconductor Conference Walker Medal, the IEEE Third Millennium Medal, and the Alexander von Humboldt Senior Research Prize in 1998 for his contributions to GaAs devices and technology.